Pure & Appl. Chem., Vol. 70, No. 4, pp. 947–954, 1998.
Printed in Great Britain.

The high valent nonheme Fe_2O_2 diamond core: Comparisons with the heme ferryl

Lawrence Que, Jr.

Department of Chemistry and Center for Metals in Biocatalysis, University of Minnesota, Minneapolis, Minnesota 55455, U. S. A.

Abstract: A high-valent Fe_2O_2 diamond core structure is proposed as the key oxidizing species in the oxygen activation chemistry of nonheme diiron enzymes such as methane monooxygenase, ribonucleotide reductase, and fatty acid desaturases. Synthetic precedents serve as the basis for this hypothesis, which is consistent with recent EXAFS results on the high-valent intermediate of methane monooxygenase. The structural and reactivity features of this core are compared with those of the heme ferryl, the key oxidizing species in heme enzymes.

Carboxylate-bridged nonheme diiron active sites have emerged as a common structural motif for an increasing number of metalloenzymes that activate dioxygen (1). This class includes the hydroxylase component of methane monooxygenase (MMOH), which carries out the hydroxylation of methane and other alkanes (2), the R2 protein of ribonucleotide reductase (RNR R2), which generates the Tyr122 radical essential for the deoxygenation of ribonucleotides (3), and fatty acid desaturases, which convert saturated fatty acids to their unsaturated derivatives (4). X-ray structures of the reduced forms of MMOH, RNR R2, and the stearoyl-acyl carrier protein Δ^9-desaturase (Δ9D) are now available and show that the diiron(II) active sites are remarkably similar (Fig. 1). Each diiron(II) unit is bridged by two

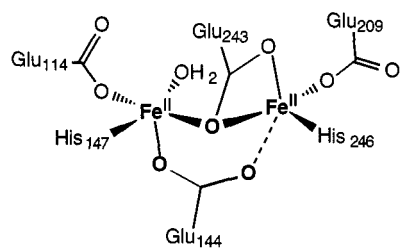

methane monooxygenase hydroxylase component

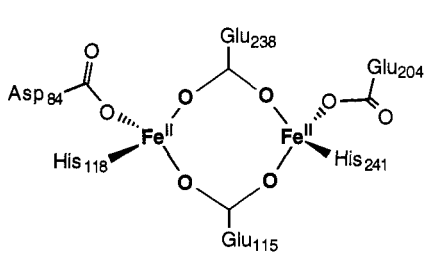

ribonucleotide reductase R2 protein

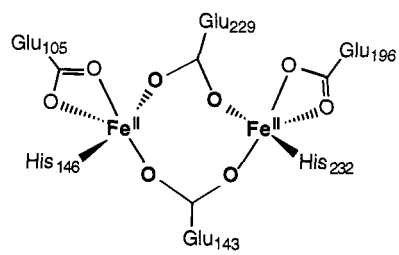

fatty acid desaturase

Fig. 1. Nonheme diiron(II) active sites of MMOH, RNR R2, and Δ9D as determined by x-ray crystallography (from refs 2-4).

carboxylate groups and terminally ligated by two His and two carboxylate residues. Furthermore, each bridging carboxylate is separated from a terminal His ligand by two residues. Indeed this D/E-X-X-H sequence is becoming the motif that characterizes this class of nonheme diiron enzymes. Such sequence motifs have been found for a number of arene hydroxylases which are likely to belong to this class as well (5). It would thus appear that this common nonheme diiron active site can carry out a range of oxidative transformations that may rival in versatility those that occur at heme active sites.

The paradigm for oxygen activation by a metalloenzyme active site is the mechanism generally accepted for heme enzymes such as cytochrome P450 and heme peroxidases (Fig. 2) (6). The activation of O_2 by the heme center is believed to result in the formation of a formally Fe^{V}=O species that is responsible for carrying out the hydroxylation of alkanes and the epoxidation of olefins. Though such a species has not been observed *per se* in the cytochrome P450 cycle, the analogous species has been characterized for heme peroxidases. This Fe^{V}=O species, called Compound I, is in fact better described as an oxoiron(IV) complex with a one-electron oxidized porphyrin ligand, so the two oxidizing equivalents implied by the Fe^{V} formalism are shared by the metal center and the porphyrin. In the peroxidase cycle, Compound I is reduced by one electron to Compound II, described as an oxoiron(IV) porphyrin complex, and then by a second electron to re-generate the starting iron(III) state. Thus, among heme enzymes, peroxidases carry out one-electron oxidations of substrates, while cytochromes P450 catalyze two-electron oxidations.

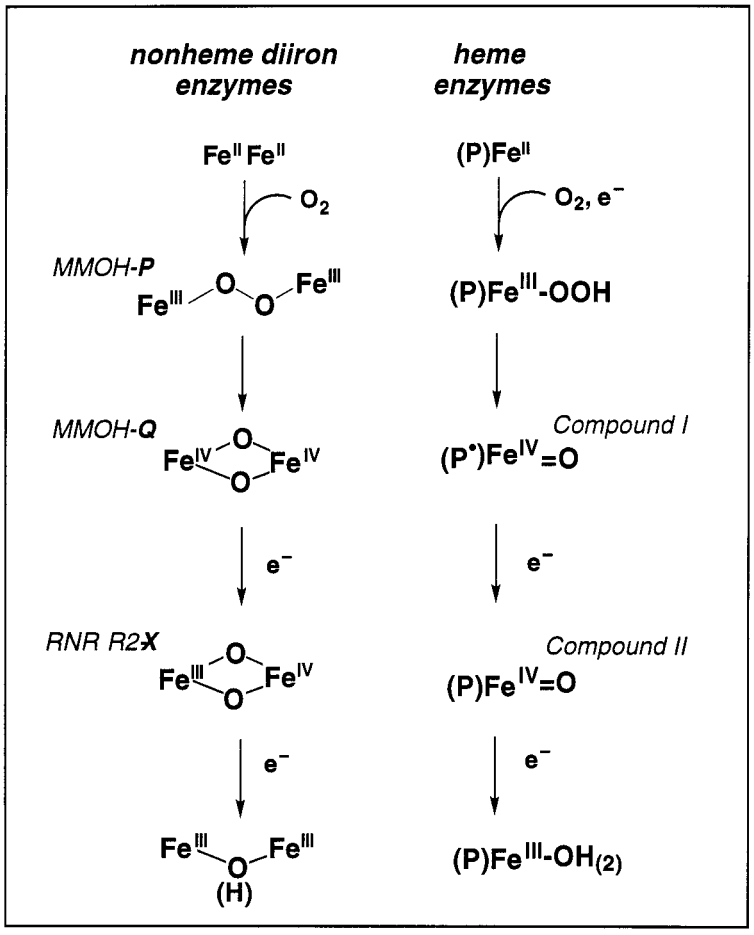

Fig. 2. Comparison of mechanistic schemes for oxygen activation by iron centers in heme and nonheme diiron enzymes.

Perhaps the most important question that arises in adapting this paradigm to the nonheme diiron enzymes is what replaces the porphyrin ligand in the high valent chemistry. We have proposed that the second iron in the active site may serve the role of the porphyrin as the repository of the second oxidizing equivalent (Fig. 2) (7). This notion is indeed borne out by rapid kinetic studies of the reaction of O_2 with diiron(II) forms of the nonheme enzymes. For MMOH, an intermediate called **Q** has been observed, which is characterized to have the diiron(IV) oxidation state and kinetically competent to hydroxylate methane (8,9). For RNR R2, an intermediate called **X** has been found and characterized to an iron(III)iron(IV) oxidation state; **X** is responsible for the oxidation of Tyr122 to its radical form (10). Thus in the mechanistic scheme shown in Fig. 2, MMOH-**Q** is analogous to heme peroxidase Compound I, while RNR R2-**X** corresponds to Compound II. In this scheme then, MMOH and Δ9D are the nonheme diiron equivalents of cytochrome P450 capable of catalyzing two-electron oxidations of hydrocarbon substrates. This analogy implies that a nonheme diiron(IV) intermediate has comparable reactivity to an oxoiron(IV) porphyrin radical species. Heme peroxidases, on the other hand, catalyze one-electron oxidations of electron-rich aromatics. The nonheme counterpart is the R2 protein of RNR, the function of which is to oxidize Tyr122 to its catalytically essential radical form.

The scheme in Fig. 2 proposes an $Fe_2(\mu\text{-}O)_2$ diamond core structure for the high-valent intermediates in the mechanisms of nonheme diiron enzymes. This idea is based on synthetic precedent. We have thus far found the only class of synthetic high-valent complexes of relevance to the chemistry of nonheme diiron enzymes, and these complexes have been found to possess $Fe_2(\mu\text{-}O)_2$ diamond core structures. These $[Fe_2(\mu\text{-}O)_2(L)_2]^{3+}$ complexes (Fig. 3; **1**, L = TPA (tris(2-pyridylmethyl)amine); **2**, L = 5-Me_3-TPA (tris(5-methyl-2-pyridylmethyl)amine); **3**, L = 6-Me-TPA ((6-methyl-2-pyridylmethyl)-bis(2-pyridylmethyl)amine)) result from the reaction of H_2O_2 and $[Fe^{III}_2(\mu\text{-}O)(L)_2(\mu\text{-}H_3O_2)]^{3+}$ and are stable enough to be characterized only at low temperature (-40 °C) (11,12). No crystal structure is available, so the structures of these complexes have been established by spectroscopic methods.

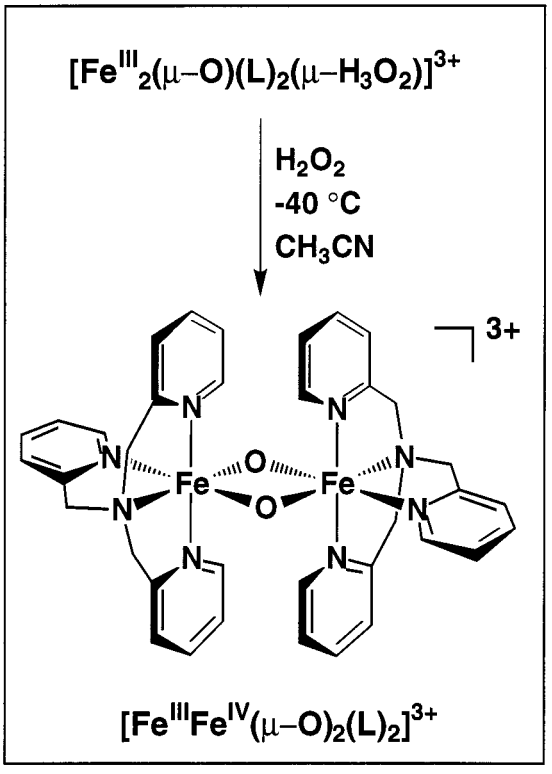

Fig. 3. Reaction to form the $[Fe_2(\mu\text{-}O)_2]^{3+}$ diamond core.

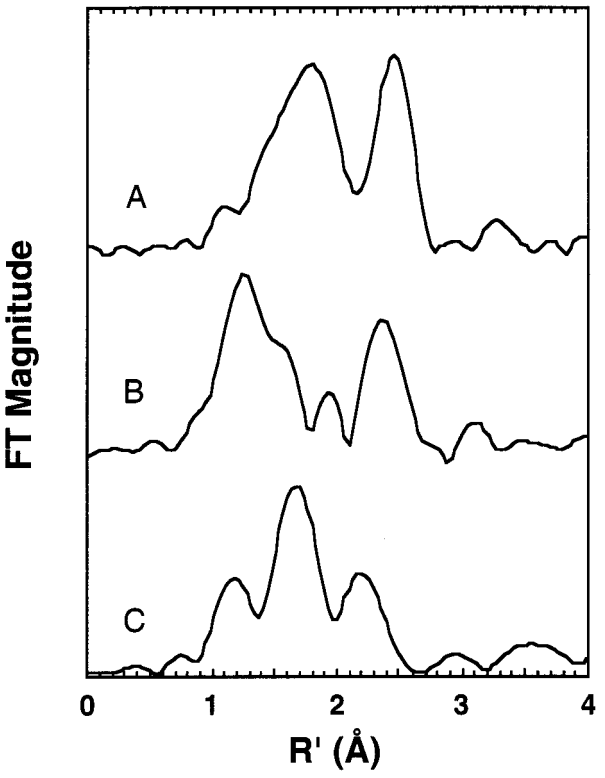

Fig. 4. Comparison of the R'-space EXAFS spectra of A) $[Fe_2O_2(6\text{-}Me_3\text{-}TPA)_2](ClO_4)_2$ (**4**), B) $[Fe_2O_2(5\text{-}Me_3\text{-}TPA)_2](ClO_4)_3$ (**2**), and C) MMOH-**Q** (61%)

Two techniques have been particularly useful: electrospray ionization mass spectrometry and EXAFS (11). The mild ionization conditions of the former allowed the molecular composition of the thermally sensitive high-valent species to be determined as $[Fe_2O_2(L)_2](ClO_4)_3$; this conclusion was based on the observed m/z values and isotope distribution patterns of positive and negative ion clusters associated with the molecular ions (11,12). EXAFS analysis of $[Fe_2O_2(5\text{-}Me_3\text{-}TPA)_2](ClO_4)_3$ showed two prominent features in its R'-space spectrum (Fig. 4B), one at ca. 1.4 Å corresponding to the first coordination sphere and another at ca. 2.4 Å corresponding to the second coordination sphere. The best fit to the first coordination sphere feature consists of 1 O @ 1.77 Å, 3 N/O @ 1.94 Å, and 2 N @ 2.17 Å (11). But it is the second coordination feature that associates these complexes with an $Fe_2(\mu\text{-}O)_2$ diamond core. This feature is best fit with an Fe scatterer at 2.9 Å. The unusually intense scattering observed suggests that this scatterer must have only a limited vibrational disorder, which we have attributed to the presence of the two single-atom bridges. Similarly intense second shell features have been observed in the EXAFS spectra of other complexes with $M_2(\mu\text{-}O)_2$ cores (13,14) including $[Fe^{III}_2O_2(6\text{-}Me_3\text{-}TPA)_2](ClO_4)_2$ (**4**) (Fig. 4A), the only example of a crystallographically characterized complex with an $Fe_2(\mu\text{-}O)_2$ diamond core (15).

The $Fe_2(\mu\text{-}O)_2$ diamond cores of **2** and **4** are compared in Fig. 5. X-ray crystallography shows the core of **4** to be centrosymmetric (15), but the oxo bridges are asymmetrically disposed between the iron ions. The two Fe-μ-O bonds of each Fe-μ-O-Fe fragment are 1.84 and 1.92 Å, with the shorter bond trans to the more weakly bonded amine nitrogen. A similar structure has been deduced for the diamond core of **2** (11). Complex **2** exhibits only one type of iron site (δ = 0.14 mm/s) in both its low and high temperature Mössbauer spectra, indicating that the two iron ions are identical despite the fact that the core has a

formal $Fe^{III}Fe^{IV}$ oxidation state (11). To date the best electronic description for this complex consistent with the available spectroscopic and magnetic data involves a valence delocalized $Fe^{III}Fe^{IV}$ center with both ions having low spin configurations. The short Fe-O bond of 1.77 Å in the EXAFS analysis is assigned to the oxo bridge trans to the amine nitrogen, while the longer Fe-O_{oxo} bond is included in the 1.94 Å shell. This significant asymmetry of the oxo bridge appears characteristic of the $Fe_2(\mu\text{-}O)_2$ core and is not observed in the cores of related $Mn_2(\mu\text{-}O)_2$ (13) and $Cu_2(\mu\text{-}O)_2$ complexes (14,16). The Fe-Fe separations of 2.9 and 2.7 Å for **2** and **4**, respectively, are comparable to those observed for $Mn_2(\mu\text{-}O)_2$ and $Cu_2(\mu\text{-}O)_2$ (2.6-2.8 Å) complexes. But it is puzzling why the Fe-Fe distance for the higher-valent **2** should be longer than that found in **4**.

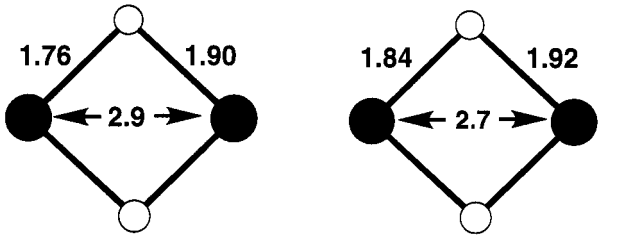

$[Fe_2O_2(5\text{-}Me_3\text{-}TPA)_2]^{3+}$ (2)

$[Fe_2O_2(6\text{-}Me_3\text{-}TPA)_2]^{2+}$ (4)

Fig. 5. Comparison of core structures of **2** and **4**.

The distinctive EXAFS features of the $Fe_2(\mu\text{-}O)_2$ diamond core have prompted us to investigate whether such features may also be associated with the high-valent intermediate **Q** of MMOH. Since MMOH-**Q** cannot be generated in quantitative yield and EXAFS analysis provides an average of all the metal environments present in the sample, it was necessary to use Mössbauer spectroscopy to determine the relative populations of the various iron species present in the samples. Thus tandem rapid-freeze-quench Mössbauer/EXAFS experiments were carried out on MMOH-**Q** (17). The R'-space EXAFS spectrum of a sample containing 61% MMOH-**Q** (Fig. 4C) shows three features at 1.2, 1.7, and 2.2 Å, corresponding to a coordination environment about each iron of 0.6 O atom at 1.77 Å, 4 O/N atoms at 2.04 Å, and 0.6 Fe atom at 2.5 Å, respectively. The other components of the sample are $MMOH_{red}$ and $MMOH_{ox}$, both of which contribute only to the 2.04 Å peak. The 1.77 Å Fe-O bond and the 2.5 Å Fe-Fe distance are thus features unique to MMOH-**Q**.

The intense 2.5 Å peak in the EXAFS spectrum of MMOH-**Q** is reminiscent of those observed for **2** and **4** (Fig. 4). While the presence of this feature does not necessarily prove that the high-valent intermediate must have an $Fe_2(\mu\text{-}O)_2$ diamond core, it does require an iron scatterer 2.5 Å from the other iron with at least two single atom bridges to account for the intensity of the scattering. To date the only precedent in iron chemistry for such a short distance is the mixed valence diiron(II,III) complex $[Fe_2(\mu\text{-}OH)_3(Me_3TACN)_2]^{2+}$ which has three hydroxo bridges that enforce an Fe-Fe distance of 2.5 Å (18). Since **2** and **4** have Fe-Fe distances longer than 2.5 Å, a third bridge must be added to the $Fe_2(\mu\text{-}O)_2$ core to decrease the Fe-Fe distance to the appropriate value. A logical candidate is a carboxylate bridge, which is present in all of the crystallographically determined active sites of MMOH (Glu144) (2) and RNR R2 (Glu115) (3,19). In support of this proposed structure, the typical Mn-Mn distance of 2.7 Å in complexes with $Mn_2(\mu\text{-}O)_2$ cores is shortened to ca. 2.6 Å upon addition of a bidentate carboxylate bridge (20).

The EXAFS analysis of MMOH-**Q** finds only one short Fe-O bond per Fe at 1.77 Å (17). This observation is consistent with the presence of a symmetric Fe-O-Fe unit that is supported by two other bridges as shown in Fig. 6A. It can also be interpreted to indicate the presence of an $Fe_2(\mu\text{-}O)_2$ unit with a core asymmetry like that found for **2** and **4** as shown in Fig. 6B. We have favored the latter structure for MMOH-**Q**, because the $Fe_2(\mu\text{-}O)_2$ diamond core is the only structure thus far demonstrated to

support the Fe^{IV} oxidation state in a nonheme ligand environment (7b,11,12). A similar conclusion was reached completely independently by Siegbahn and Crabtree (21), who carried out density functional theory calculations on the various components of the MMOH catalytic cycle. Indeed the core dimensions predicted by the calculations for MMOH-**Q** closely matched the experimentally obtained values.

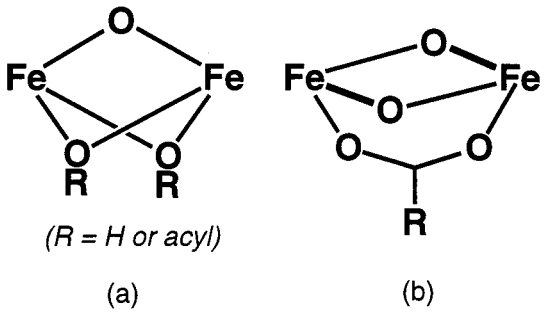

Fig. 6. Possible core structures consistent with the EXAFS analysis for MMOH-**Q**.

The $Fe_2(\mu\text{-}O)_2$ core proposed for MMOH-**Q** at first glance differs significantly from the mononuclear high-valent iron-oxo unit associated with heme peroxidase Compounds I and II (6). Though heme and nonheme intermediates possess characteristic short Fe-O bonds, those of the heme intermediates are at least 0.1 Å shorter (22). We propose however the core asymmetry observed for the $Fe_2(\mu\text{-}O)_2$ diamond core could be construed as the result of the head-to-tail dimerization of two Fe=O monomers (Fig. 6B). The additional interactions from the bridging arrangement would then serve to stabilize the Fe^{IV} oxidation state in a nonheme ligand environment.

Reactivity studies demonstrate that the high-valent $Fe_2(\mu\text{-}O)_2$ core can effect oxidations similar to those carried out by MMOH, RNR R2, and Δ9D (23). Detailed information is thus far available only for $[Fe_2(\mu\text{-}O)_2(TPA)_2]^{3+}$ (**1**). For example, **1** acts as a one-electron oxidant to oxidize 2,4-di-*tert*-butylphenol quantitatively to its phenoxy radical within seconds and is reduced to a (μ-oxo)diiron(III) species, i. e.

$$[Fe_2(\mu\text{-}O)_2(TPA)_2]^{3+} + PhOH \rightarrow [Fe_2(\mu\text{-}O)(\mu\text{-}OH)(TPA)_2]^{3+} + PhO\bullet$$

This reaction thus models the oxidation of Tyr122 by RNR-R2 **X** in the assembly of the diiron(III)-tyrosyl radical cofactor found in active RNR R2 (9). Complex **1** also oxidizes cumene, resulting in the hydroxylation of the tertiary C-H bond or the desaturation of the isopropyl group (Fig. 7) (21). These

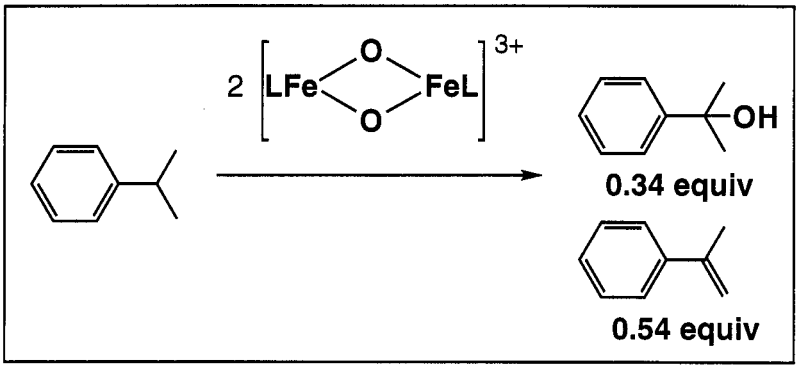

Fig. 7. Oxidation of cumene by **1**.

transformations are analogous to reactions catalyzed by MMO and fatty acid desaturases. Since **1** is only a one-electron oxidant, two equivalents are required per product molecule formed, and substrate oxidation must occur in two steps. We have found that the first and rate determining step is the formation of an intermediate benzylic radical; this is indicated by results from O_2 trapping experiments and confirmed by the observation of a kinetic isotope effect of 20 in the reaction of **1** with ethylbenzene or ethylbenzene-d_{10} at -40 °C. The second step involves the reaction of the intermediate benzylic radical with another molecule of **1** forming either the alcohol or the olefin. The factors that determine the alcohol/olefin product ratio are under investigation.

Somewhat disappointingly, benzylic C-H bonds are the strongest C-H bonds that are attacked by **1**. However this should not be too surprising, since **1** is formally in the iron(III)iron(IV) oxidation state or analogous to Compound II of heme enzymes. When considered in this light, the reactivity of **1** toward hydrocarbon substrates appears to be flanked by those of oxoiron(IV) porphyrin radical complexes and their one-electron reduced counterparts. Oxoiron(IV) porphyrin radical complexes analogous to Compound I are two-electron oxidants which are capable of hydroxylating alkanes including cyclohexane (24). In contrast, oxoiron(IV) porphyrin complexes are one-electron oxidants and capable only of abstracting hydrogen atoms from allylic C-H bonds (25). Thus a species in the diiron(IV) oxidation state would presumably have the higher potential to enable it to abstract a hydrogen atom from stronger C-H bonds. Furthermore **1** can carry out the desaturation of alkanes, a reaction that has not been reported for a synthetic iron porphyrin complex. Perhaps this is a reactivity that is unique to the $Fe_2(\mu\text{-}O)_2$ diamond core.

In summary, synthetic precedents for the $Fe_2(\mu\text{-}O)_2$ diamond core are now available. Though having a somewhat limited oxidizing power, an $Fe_2(\mu\text{-}O)_2$ complex has been found to display a versatile oxidative reactivity that encompasses the range of reactions catalyzed by the nonheme diiron enzymes. This versatility supports the notion illustrated in Fig. 2 that a high valent species with an $Fe_2(\mu\text{-}O)_2$ diamond core (or some variation thereof) may be the common feature of the oxidative mechanisms of this family of enzymes, a notion supported by recent EXAFS studies of intermediate **Q** of MMOH (17).

Acknowledgments

Our work has been generously supported by the National Institutes of Health (GM-38767) and the National Science Foundation (MCB-9405723).

References

1. (a) B. J. Wallar and J. D. Lipscomb. *Chem. Rev.* **96**, 2625-2657 (1996).
   (b) A. L. Feig and S. J. Lippard. *Chem. Rev.* **94**, 759-805 (1994).
   (c) L. Que, Jr. In *Bioinorganic Catalysis* (J. Reedijk, ed.), pp 347-393. Marcel Dekker, New York (1993).
2. (a) A. C. Rosenzweig, C. A. Frederick, S. J. Lippard, and P. Nordlund. *Nature* **366**, 537-543 (1993).
   (b) A. C. Rosenzweig, P. Nordlund, P. M. Takahara, C. A. Frederick, and S. J. Lippard. *Chem. Biol.* **2**, 409-418 (1995).
   (c) N. Elango, R. Radhakrishnam, W. A. Froland, B. J. Wallar, C. A. Earhart, J. D. Lipscomb, and D. H. Ohlendorf. *Protein Sci.* **6**, 556-568 (1997).
3. (a) P. Nordlund and H. Eklund. *J. Mol. Biol.* **232**, 123-164 (1993).
   (b) D. T. Logan, X.-D. Su, A. Åberg, K. Regnström, J. Hajdu, H. Eklund, and P. Nordlund. *Structure* **4**, 1053-1064 (1996).
4. Y. Lindqvist, W. Huang, G. Schneider, and J. Shanklin. *EMBO J.* **15**, 4081-4092 (1996).
5. J. D. Pikus, J. M. Studts, C. Achim, K. E. Kauffmann, E., Münck, R. J. Steffan, K. McClay, and B. G. Fox. *Biochemistry* **35**, 9106-9119 (1996).
6. J. H. Dawson. *Science* **240**, 433-439 (1988).

7. (a) L. Que, Jr. *Science* **253**, 273-274 (1991).
(b) L. Que, Jr. and Y. Dong. *Acc. Chem. Res.* **29**, 190-196 (1996).
8. (a) S.-K. Lee, J. C. Nesheim, and J. D. Lipscomb. *J. Biol. Chem.* **268**, 21569-21577 (1993).
(b) S.-K. Lee, B. G. Fox, W. A. Froland, J. D. Lipscomb, and E. Münck. *J. Am. Chem. Soc.* **115**, 6450-6451 (1993).
9. (a) K. E. Liu, D. Wang, B. H. Huynh, D. E. Edmondson, A. Salifoglou, and S. J. Lippard. *J. Am. Chem. Soc.* **116**, 7465-7466 (1994).
(b) K. E. Liu, A. M. Valentine, D. Wang, B. H. Huynh, D. E. Edmondson, A. Salifoglou, and S. J. Lippard. *J. Am. Chem. Soc.* **117**, 10174-10185 (1995).
10. (a) J. M. Bollinger, Jr., D. E. Edmondson, B. H. Huynh, J. Filley, J. Norton, and J. Stubbe. *Science* **253**, 292-298 (1991).
(b) N. Ravi, J. J. M. Bollinger, B. H. Huynh, D. E. Edmondson, and J. Stubbe. *J. Am. Chem. Soc.* **116**, 8007-8014. (1994).
(c) W. H. Tong, S. Chen, S. G. Lloyd, D. E. Edmonson, B. H. Huynh, and J. Stubbe. *J. Am. Chem. Soc.* **118**, 2107-2108 (1996).
(d) B. E. Sturgeon, D. Burdi, S. Chen, B.-H. Huynh, D. E. Edmondson, J. Stubbe, and B. M. Hoffman. *J. Am. Chem. Soc.* **118**, 7551-7557 (1996).
11. Y. Dong, H. Fujii, M. P. Hendrich, R. A. Leising, G. Pan, C. R. Randall, E. C. Wilkinson, Y. Zang, L. Que, Jr., B. G. Fox, K. Kauffmann, and E. Münck. *J. Am. Chem. Soc.* **117**, 2778-2792 (1995).
12. Y. Dong, L. Que, Jr., K. Kauffmann, and E. Münck. *J. Am. Chem. Soc.* **117**, 11377-11378 (1995).
13. (a) V. K. Yachandra, K. Sauer, and M. P. Klein. *Chem. Rev.* **96**, 2927-2950 (1996).
(b) R. Manchanda, G. W. Brudvig, and R. H. Crabtree. *Coord. Chem. Rev.* **144**, 1-38 (1995).
14. S. Mahapatra, J. A. Halfen, E. C. Wilkinson, G. Pan, X. Wang, V. G. Young, Jr., C. J. Cramer, L. Que, Jr., and W. B. Tolman. *J. Am. Chem. Soc.* **118**, 11555-11574 (1996).
15. Y. Zang, Y. Dong, L. Que, Jr., K. Kauffmann, and E. Münck. *J. Am. Chem. Soc.* **117**, 1169-1170 (1995).
16. S. Mahapatra, V. G. Young, Jr., S. Kaderli, A. D. Zuberbühler, and W. B. Tolman. *Angew. Chem. Int. Ed. Engl.* **36**, 130-133 (1997).
17. L. Shu, J. C. Nesheim, K. Kauffmann, E. Münck, J. D. Lipscomb, and L. Que, Jr. *Science* **275**, 515-518 (1997).
18. (a) D. R. Gamelin, E. Bominaar, M. L. Kirk, K. Wieghardt, and E. I. Solomon. *J. Am. Chem. Soc.* **118**, 8085-8097 (1996).
(b) X.-Q. Ding, E. L. Bominaar, E. Bill, H. Winkler, A. X. Trautwein, S. Drüeke, P. Chaudhuri, and K. Wieghardt. *J. Chem. Phys.* **92**, 178-186 (1990).
19. (a) M. Atta, P. Nordlund, A. Åberg, H. Eklund, and M. Fontecave. *J. Biol. Chem.* **26**, 20682-20688 (1992)
(b) A. Åberg, M. Ormö, P. Nordlund, and B.-M. Sjöberg. *Biochemistry* **32**, 9845-9850 (1993).
20. (a) K. Wieghardt, U. Bossek, B. Nuber, J. Weiss, J. Bonvoisin, M. Corbella, S. E. Vitols, and J.-J. Girerd. *J. Am. Chem. Soc.* **110**, 7398-7411 (1988).
(b) S. Pal, J. W. Gohdes, W. C. A. Wilisch, and W. H. Armstrong. *Inorg. Chem.* **31**, 713-716 (1992).
21. P. Siegbahn and R. H. Crabtree. *J. Am. Chem. Soc.* **119**, 3103-3113 (1997).
22. J. E. Penner-Hahn, K. S. Eble, T. J. McMurry, M. Renner, A. L. Balch, J. T. Groves, J. H. Dawson, and K. O. Hodgson. *J. Am. Chem. Soc.* **108**, 7819-7825 (1986).
23. C. Kim, Y. Dong, and L. Que, Jr. *J. Am. Chem. Soc.* **119**, 3635-3636 (1997).
24. T. J. McMurry and J. T. Groves. In *Cytochrome P-450. Structure, Mechanism, and Biochemistry* (P. R. Ortiz de Montellano, ed.), pp. 1-28. Plenum Press, New York (1986).
25. M.-h. Liu, C.-y. Yeh, and Y. O. Su. *J. Chem.Soc., Chem. Commun.* 1437-1438 (1996).